JJEE
Volume 6, Number 1, 2020
Pages 35-48
Jordan Journal of Electrical Engineering
ISSN (Print): 2409-9600, ISSN (Online): 2409-9619

A Mathematical Morphology-Based Fault Detection and Faulty Phase Categorization Scheme for the Protection of Six-Phase Transmission Line

Gaurav Kapoor*

Department of Electrical Engineering, Modi Institute of Technology, Kota, India
E-mail: gaurav.kapoor019@gmail.com

Received: October 25, 2019 *Revised: November 11, 2019* *Accepted: November 16, 2019*

***Abstract*—** This paper proposes a fault recognition and faulty phase categorization technique – based on mathematical morphology (MM) - for the protection of six-phase transmission line (SPTL). The single side captured fault currents of the SPTL are used to evaluate the amplitudes of MM coefficients (Boucher gradient). To validate the performance of the proposed technique, an extensive collection of test studies are executed by varying fault type, location, resistance, and switching time. The value of fault resistance is varied from 5 Ω to 60 Ω, the value of ground resistance is varied from 5 Ω to 45 Ω and the location of fault is varied from 25 km to 50 km. The results show that MM correctly detects all types of faults in SPTL by employing one-side fault current data only and that the proposed scheme is robust to the variation in the fault factors of SPTL.

***Keywords*—** Fault detection; Fault categorization; Mathematical morphology; Six-phase transmission line protection.

1. INTRODUCTION

A raise in the certainty of electrical power has been perceived by the citizens of the modern generation. The electrical power transfer potentiality of the currently operating power transmission systems ought to be augmented in order to assist the significant increase in the necessity of electrical energy. In the literature, six-phase transmission lines (SPTL) have been suggested as an imminent replacement of the prevalent configuration of the electrical power transmission system which has the prospective for transferring the large extent of electrical energy.

The feasibility of fault occurrence on the SPTL is more when comparing with double circuit transmission line. Thus, accurate detection of the faults in the SPTL turns out to be very decisive for mitigating the loss of gain and providing fast renovates.

Several newly reported research works addressed the issue related to fault recognition and categorization in SPTL. Some important research attempts are presented in concise here in this section. Kapoor employed the Hilbert-Huang transform (HHT) to detect and classify three-phase to ground faults in SPTL [1]. Ashok and Yadav reported a fault detection and classification scheme - during power swing - using maximum overlap discrete wavelet transform (MODWT) [2]. HHT based single-line to ground far-end and close-in fault detection and classification has been demonstrated for SPTL by Kapoor [3]. Shukla et al. adopted artificial neural network (ANN) and decision tree (DT) based protection technique for SPTL to explore the power quality information [4]. Further, Kapoor utilized the discrete Walsh Hadamard transform (DWHT) for fault detection [5]. The HHT is employed to detect and classify four-phase to ground faults in SPTL [6]. Kapoor carried out fault recognition in

* Corresponding author
Article's DOI: 10.5455/jjee.204-1581015401

fifteen-phase transmission line using daubechies-4 wavelet transform (Db4WT) [7]. Kapoor presented a three-phase to ground multi-position fault detection and classification algorithm for twelve-phase transmission line using the wavelet transform (WT) [8]. An ANN has been used with WT by Koley et al for faulty zone identification and fault location in SPTL [9]. The WT has been used to detect boundary faults in SPTL [10]. Gautam et al presented a fault identification technique using WT [11]. A WT-based phase to phase fault recognition method was discussed by Kapoor [12]. Sharma et. al reported a fault detection algorithm using HHT [13]. Fault detection method base on mathematical morphology (MM) is considered for the boundary protection of SPTL [14]. In [15], fault detection has been carried out using Walsh Hadamard transform (WHT).

In this work, the MM is executed for the detection of faults and categorization of faulty phase in the SPTL. The proposed MM-based technique competency to detect the faults and the susceptibility of the MM uniformity to the deviations in the fault factors are explored.

This article is structured as following: Section 2 presents the specifications of SPTL. Section 3 describes the process of fault detection using MM. Section 4 presents the performance appraisal of the investigations achieved in this work. Section 5 concludes the article.

2. SPECIFICATIONS OF THE SIX-PHASE TRANSMISSION LINE

The planned MM-based fault detection method has been executed for a 138 kV six-phase, 60 Hz, 68 km long transmission line (Springdale-McCalmont). Fig. 1 shows the schematic of proposed six-phase transmission network. At both ends of the transmission line, a 138 kV power source is connected. Two loads are also connected at the receiving end of SPTL. The SPTL is alienated into two zones with a length of 34 km each. The current measuring devices are installed at bus-1 (relaying point) of SPTL. To realize the simulation studies, this 138 kV SPTL has been designed and simulated for various types of faults in MATLAB. For each and every fault case, the fault factors are varied in order to investigate their impact on the performance of the proposed fault detection technique. The value of fault resistance is varied from 5 to Ω to 60 Ω, the value of ground resistance is varied from 5 Ω to 45 Ω and the location of fault is varied from 25 km to 50 km. The SPTL has been simulated for various types of phase to phase and phase to ground faults such as six-phase to ground fault, five-phase to ground fault, four-phase to ground fault and other conventional faults which occur on three-phase transmission line such as three-phase faults, phase to phase faults, single line to ground faults.

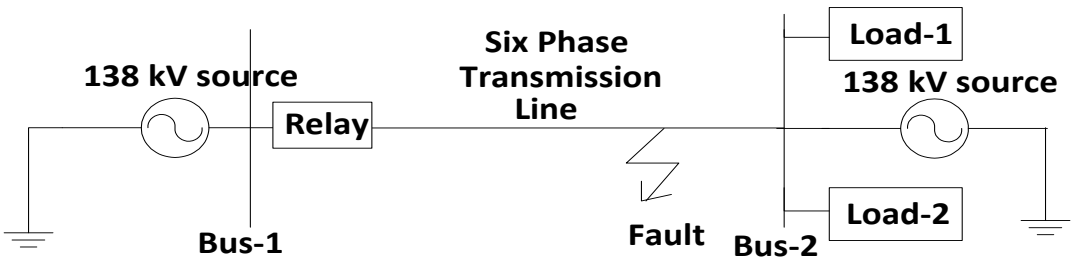

Fig. 1. Schematic of the 138 kV SPTL.

3. MM-BASED FAULT DETECTION AND FAULTY PHASE RECOGNITION SCHEME

MM is a time-domain approach having attractive features like accuracy and simplicity. It can be used for the detection, classification and location of faults in transmission lines. By the usage of different morphological filtering operations, the fault generated transient disturbances features can be easily obtained.

If f (p) is the signal then its domain $D_f = \{x_0, x_1,\ldots x_p\}$ and s (q) is the structuring element having domain $D_q = \{y_1, y_2,\ldots y_q\}$ and p > q, p and q are the integers, then the dilation of f(p) by s (q), denoted by (f⊕s) can be defined as: -

$$y_d(p) = (f \oplus s)(p) = \max\{f(p-q)+s(q),\ 0 \le (p-q) \le p, q \ge 0\} \quad (1)$$

The erosion of f (p) by s (q) denoted as (f⊖s) can be defined as: -

$$y_e(p) = (f \ominus s)(p) = \min\{f(p+q)-s(q),\ 0 \le (p+q) \le p, q \ge 0\} \quad (2)$$

In this work, MM is utilized because it decomposes the fault currents into different gradients and has many advantages over the other fault detection tools. Fig. 2 illustrates the process for the proposed MM-based fault recognition technique. The steps are shown beneath:

- Step 1: Simulate the SPTL for creating faults and produce the post-fault currents.
- Step 2: Use MM to examine the post-fault currents for characteristics retrieval.
- Step 3: Select a common threshold value for all the cases of faults by executing different types of simulation studies. In this work, a common threshold value of 1000 is selected after carrying out extensive simulation studies.
- Step 4: The phase will be proclaimed as the faulty phase and the relay will issue the trip signal when its MM Beucher gradient exceeds the threshold value.

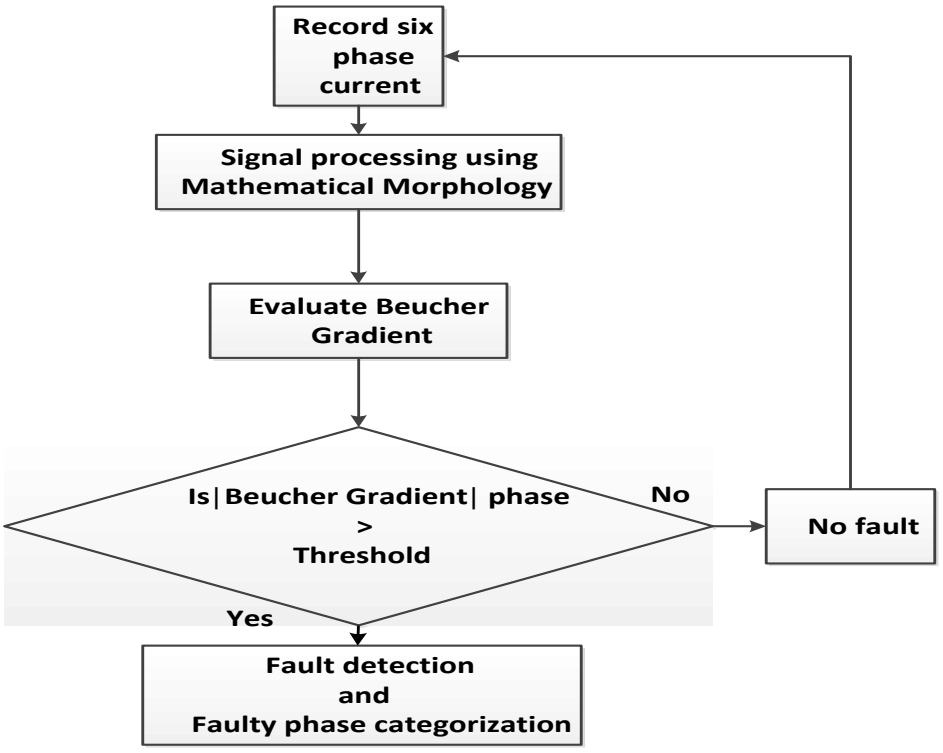

Fig. 2. The procedure of fault detection using MM.

4. PERFORMANCE APPRAISAL

The proposed MM-based scheme has been tested for different types of faults by varying the fault factors such as fault resistance (R_F), ground resistance (R_G), fault switching time (FST), and location of fault (F_L). In this work, the value of fault resistance is varied from 5 Ω to 60 Ω, the value of ground resistance is varied from 5 Ω to 45 Ω and the location of fault is varied from 25 km to 50 km. The results are revealed in the following subsections.

4.1. Effectiveness of MM for Healthy Condition

The proposed MM-based technique has been investigated for no-fault condition. Fig. 3 exhibits the six-phase currents and voltages for no-fault. Fig. 4 depicts the Beucher gradients of phase-A, B and C currents for no-fault. Fig. 5 depicts the Beucher gradients of phase-D, E and F currents for no-fault. From Figs. 4 and 5, it is observed that the Beucher gradients of six-phase currents during no-fault condition are beneath the threshold line. This means that the SPTL has no-fault. The amplitudes of Beucher gradients of six-phase currents for no-fault situation are shown in Table 1, from which it is clear that the SPTL has no-fault.

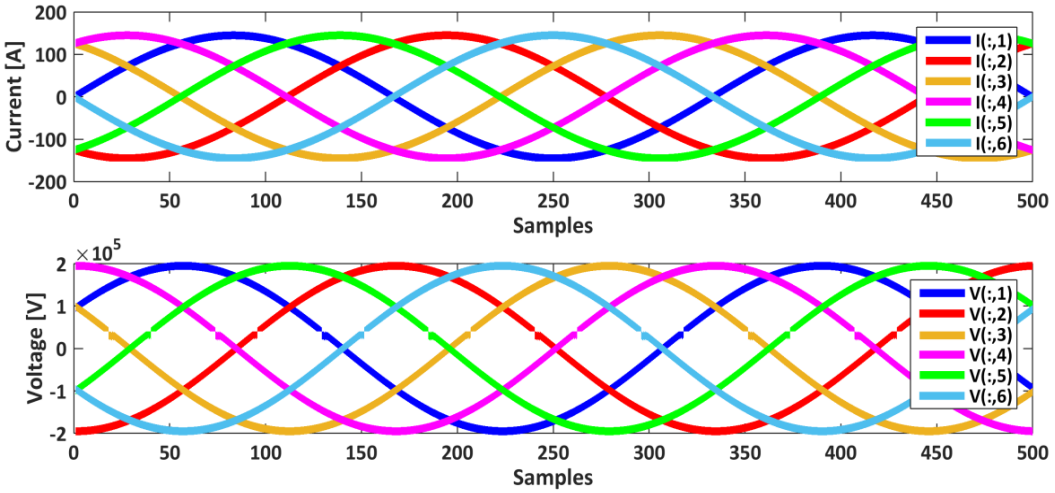

Fig. 3. Six-phase currents and voltages during no-fault.

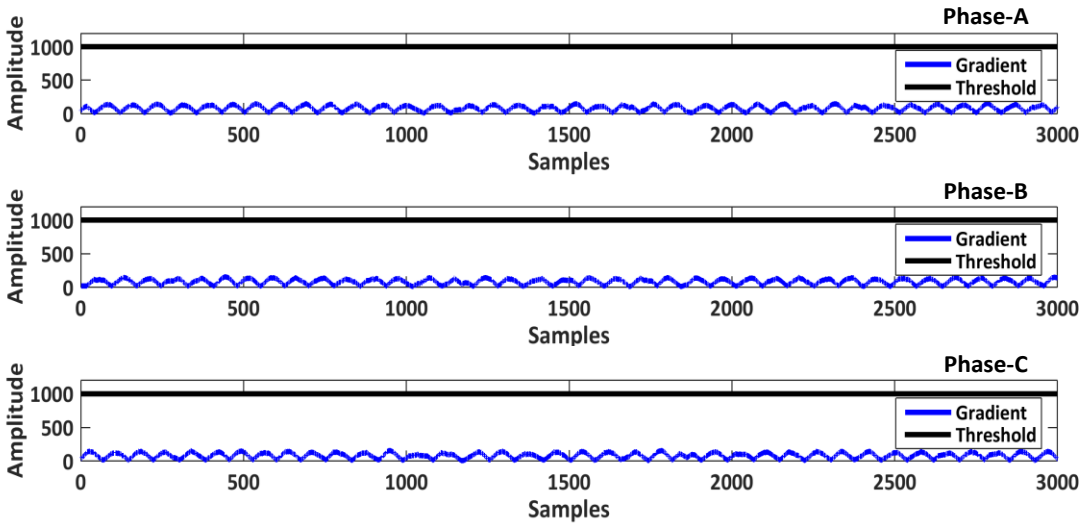

Fig. 4. Beucher gradients of phase-A, B and C currents during no-fault.

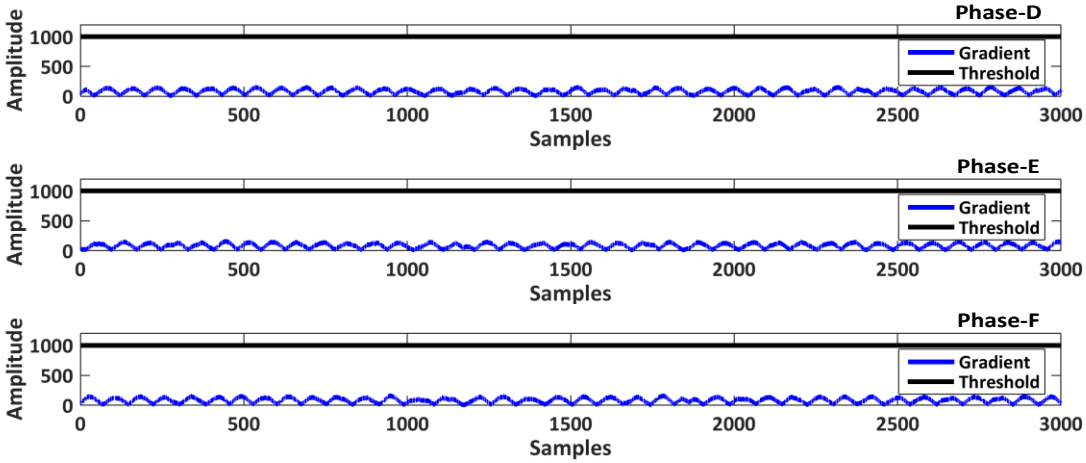

Fig. 5. Beucher gradients of phase-D, E and F currents during no-fault.

Table 1. Effectivness of MM for no-fault.

Beucher gradients					
Phase-A	Phase-B	Phase-C	Phase-D	Phase-E	Phase-F
154.4558	157.9159	165.6005	153.4540	162.3809	155.4050

4.2. Effectiveness of MM in Detecting Different Fault Types

The MM has been explored for different types of faults, simulated on SPTL. Fig. 6 depicts the six-phase currents for five-phase to ground ABCDEG fault tested at 34 km, 0.05 s R_F = 2.5 Ω and R_G = 3.5 Ω. Fig. 7 shows the Beucher gradients of phase-A, B and C currents for the ABCDEG fault. Fig. 8 shows the Beucher gradients of phase-D, E and F currents for the ABCDEG fault. The amplitudes of Beucher gradient of morphological filter of phase-A, B, C, D and E are greater than the threshold in case of ABCDEG fault as depicted in Figs. 7 and 8. The selected fault factors - which are common for all the fault cases - are: F_L = 34 km, FST = 0.05 s, R_F = 2.5 Ω and R_G = 3.5 Ω. Table 2 details the results of proposed scheme for detecting different faults. It is evident that MM perfectly detects all types of faults, simulated on the SPTL, as the amplitudes of Beucher gradient of the faulted phases are above the threshold, while the amplitudes of Beucher gradient for the healthy phases are below the threshold.

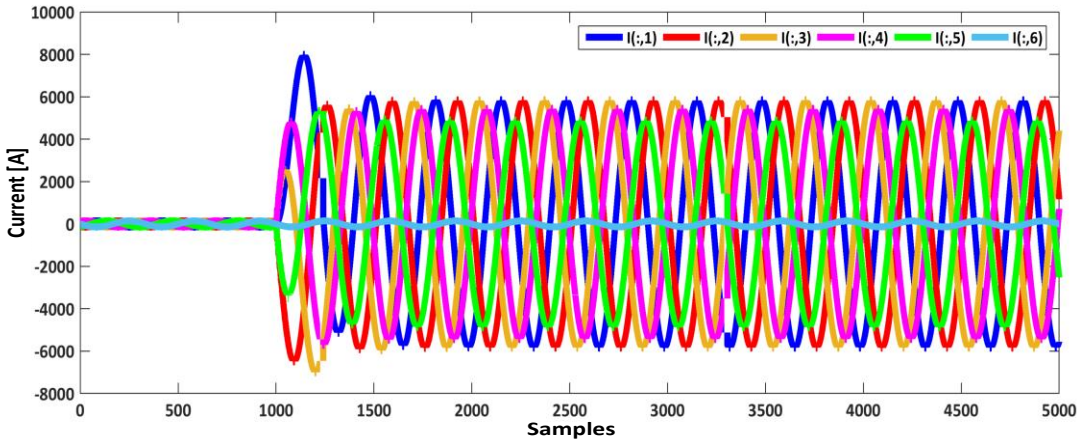

Fig. 6. Six-phase current during ABCDEG fault at 34 km, 0.05 s, R_F = 2.5 Ω and R_G = 3.5 Ω.

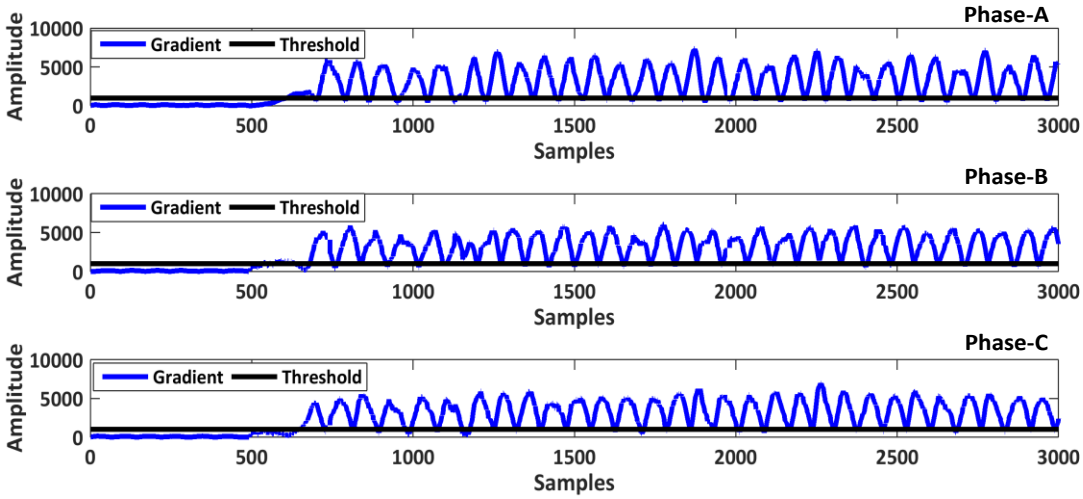

Fig. 7. Beucher gradients of phase-A, B and C currents during ABCDEG fault at 34 km, 0.05 s, R_F = 2.5 Ω and R_G= 3.5 Ω.

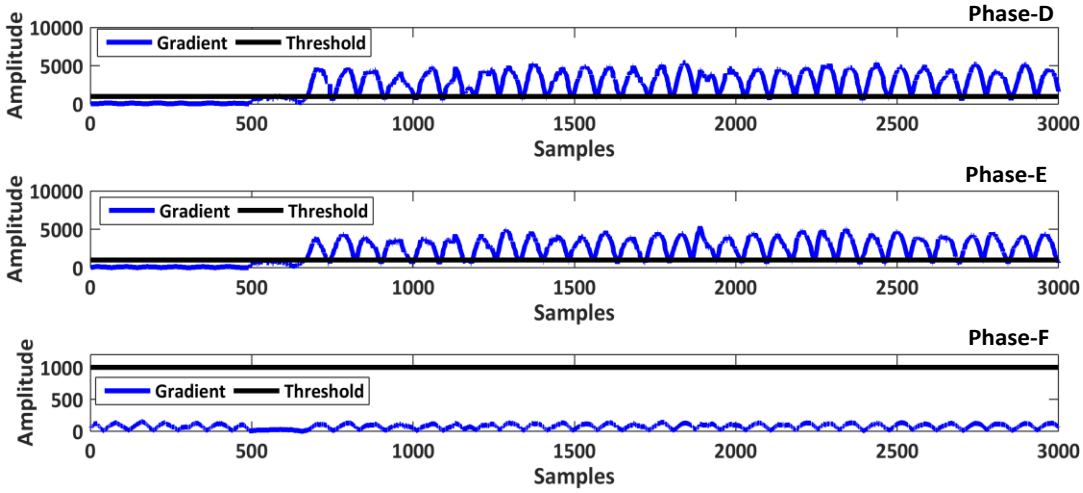

Fig. 8. Beucher gradients of phase-D, E and F currents during ABCDEG fault at 34 km, 0.05 s, R_F = 2.5 Ω and R_G = 3.5 Ω.

Table 2. Effectiveness of MM in detecting different faults

Fault type	R_F [Ω]	R_G [Ω]	Beucher gradients					
			Phase-A	Phase-B	Phase-C	Phase-D	Phase-E	Phase-F
ABCDEG	2.5	3.5	7.3113*10^3	6.3397*10^3	6.9016*10^3	5.5763*10^3	5.5898*10^3	142.9536
CDEFG	2.5	3.5	157.6957	168.5001	3.7753*10^3	5.9594*10^3	7.1395*10^3	5.9078*10^3
ABCG	2.5	3.5	6.2612*10^3	6.7760*10^3	6.1973*10^3	154.2457	151.9801	166.3013
DEF	2.5	3.5	156.2170	156.3821	156.8311	6.3271*10^3	6.4274*10^3	6.3879*10^3
ABG	2.5	3.5	5.8135*10^3	5.3919*10^3	157.8043	169.8388	152.6990	171.1580
EF	2.5	3.5	166.5239	156.4037	152.8375	158.2716	5.7473*10^3	5.4296*10^3
AG	2.5	3.5	3.3506*10^3	156.4844	157.8043	146.4060	156.4831	138.6872

4.3. Effectiveness of MM in Detecting Faults, Tested with Different Fault Resistances

The proposed MM-based scheme has been explored for detecting different types of faults - simulated on the SPTL (with and without ground) - with different values of fault resistances. Fig. 9 depicts the six-phase currents for the most rigorous fault: six-phase to

ground ABCDEFG fault simulated at 40 km, at 0.1 s, R_F = 10 Ω and R_G = 0.001 Ω. Fig. 10 exhibits the Beucher gradients of phase-A, B and C currents for the ABCDEFG fault. Fig. 11 shows the Beucher gradients of phase-D, E and F currents for the ABCDEFG fault. The amplitudes of Beucher gradient of morphological filter of all the six-phases are greater than the threshold in case of ABCDEFG (LLLLLLG) fault as shown in Figs. 10 and 11, respectively. The selected fault factors - that are common for all the fault cases - are: F_L = 40 km, FST = 0.1 s and R_G = 0.001 Ω. Table 3 shows the results of examining the effectiveness of proposed scheme in detecting different faults. It is evident that the proposed MM-based technique effectively detects all types of faults and categorizes the faulty phases, simulated on the SPTL for different fault resistances as well. Thus it is confirmed that the faults (with and without ground) with different fault resistances does not affects the performance of the proposed MM-based scheme.

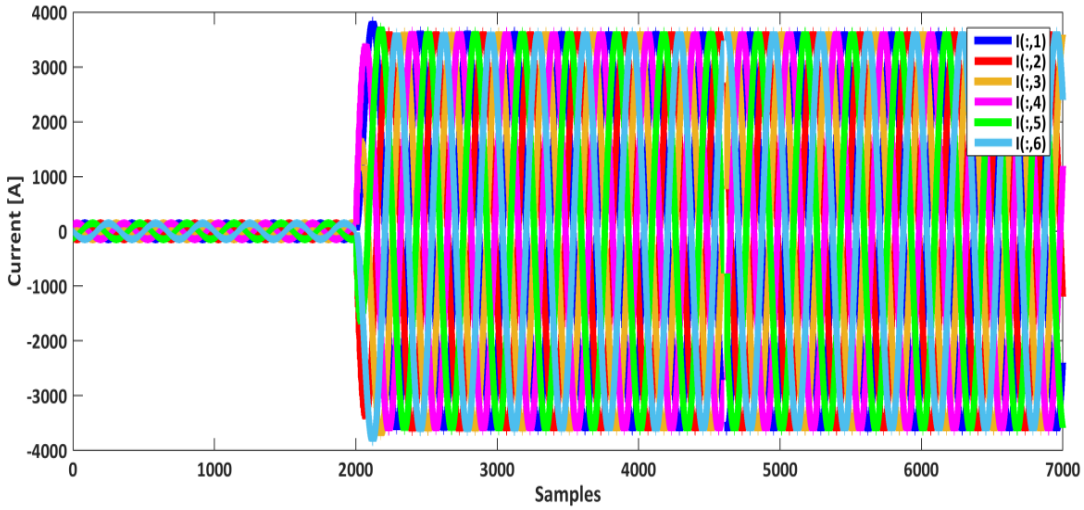

Fig. 9. Six-phase current during ABCDEFG fault at 40 km, 0.1 s, R_F = 10 Ω and R_G = 0.001 Ω.

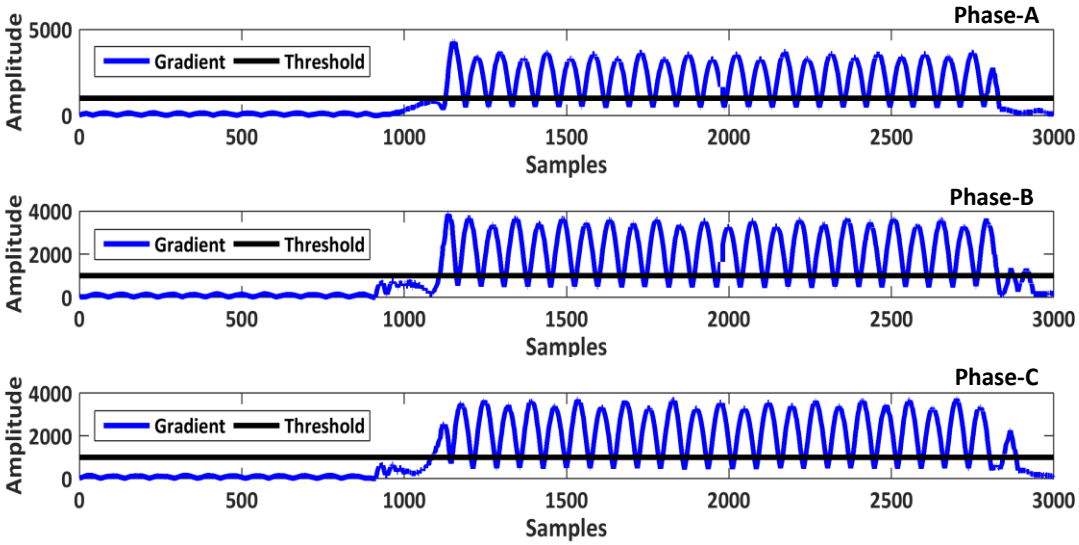

Fig. 10. Beucher gradients of phase-A, B and C currents for ABCDEFG fault at 40 km, 0.1 s, R_F = 10 Ω and R_G = 0.001 Ω.

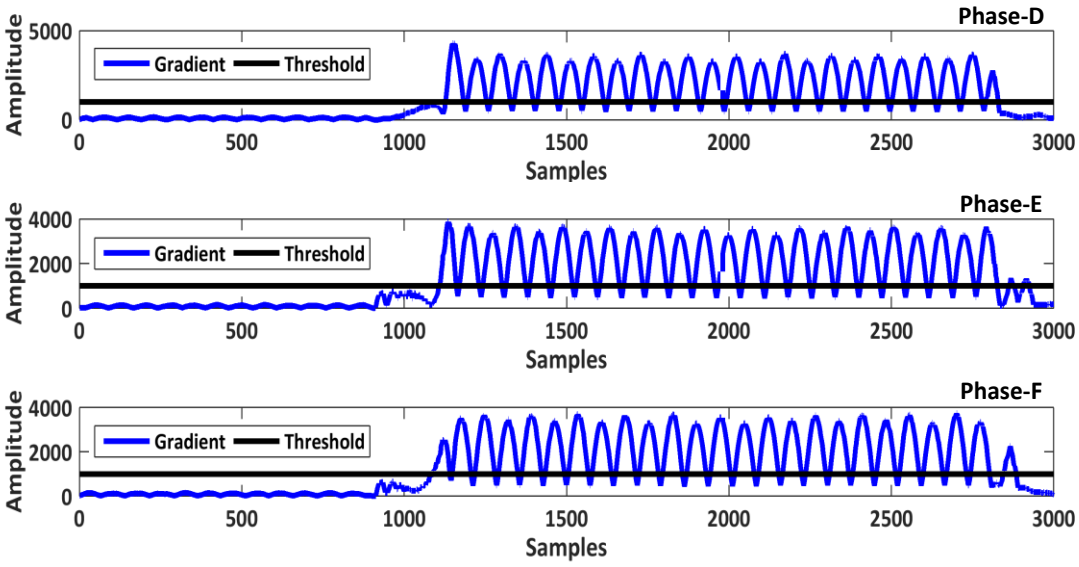

Fig. 11. Beucher gradients of phase-D, E and F currents for ABCDEFG fault at 40 km, 0.1 s, R_F = 10 Ω and R_G = 0.001 Ω.

Table 3. Effectiveness of MM in detecting faults, with different fault resistances.

Fault type	R_F [Ω]	FST [s]	Beucher gradients					
			Phase-A	Phase-B	Phase-C	Phase-D	Phase-E	Phase-F
BG	5	0.1	225.0399	3.1963*10^3	226.8241	163.0011	154.4680	162.1645
ABCDEFG	10	0.1	4.9388*10^3	4.2148*10^3	3.7523*10^3	4.4949*10^3	4.0240*10^3	4.5839*10^3
ACDE	30	0.1	1.5323*10^3	161.8751	1.6383*10^3	1.6278*10^3	1.5811*10^3	161.7735
DE	50	0.1	161.6089	159.7297	161.8372	1.0722*10^3	1.0345*10^3	163.0763
ABCG	60	0.1	1.0403*10^3	1.0736*10^3	1.0543*10^3	162.6420	163.0683	161.1069

4.4. Effectiveness of MM in detecting Faults, Tested with Different Ground Resistances

The proposed MM-based scheme has been tested for detecting different types of faults - simulated on the SPTL - with different ground resistances. Fig. 12 depicts a five-phase to ground BCDEFG fault simulated at 30 km, 0.07 s, R_G = 5 Ω and R_F = 0.001 Ω. Fig. 13 exhibits the Beucher gradients of phase-A, B and C currents for the BCDEFG fault. Fig. 14 shows the Beucher gradients of phase-D, E and F currents for the BCDEFG fault. The amplitudes of Beucher gradient of morphological filter of phase-B, C, D, E and F are greater than the threshold in case of BCDEFG (LLLLLG) fault as depicted in Figs. 13 and 14, respectively. The selected fault factors – common for all the fault cases - are: F_L = 30 km, FST = 0.07 s and R_F = 0.001 Ω. Table 4 details the results of examining the proposed scheme for detecting different faults. The simulation results, exhibited in Table 4, substantiate the effectiveness of the proposed scheme for detecting faults for different ground resistances and confirms that such faults does not affect the performance of the proposed MM-based scheme.

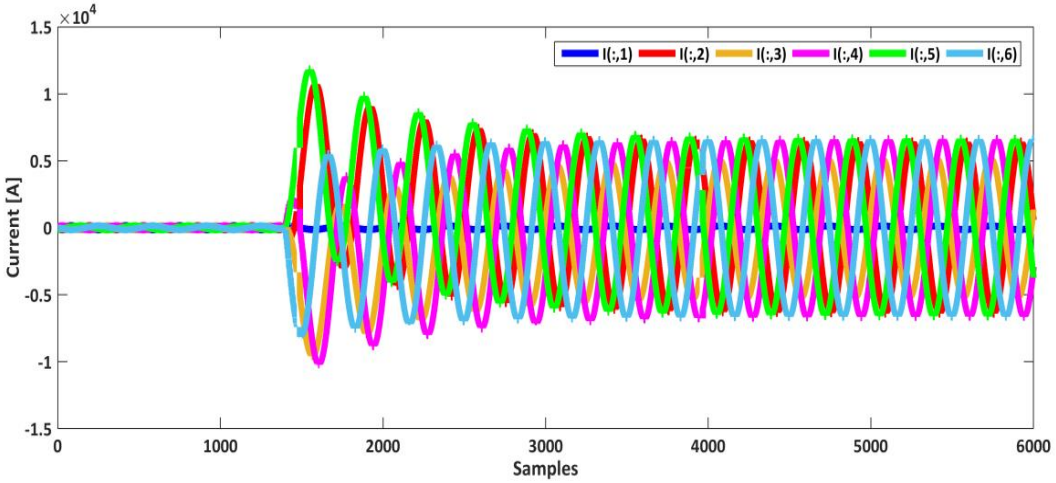

Fig. 12. Six-phase current during BCDEFG fault at 30 km, 0.07s, R_F = 0.001 Ω and R_G = 5 Ω.

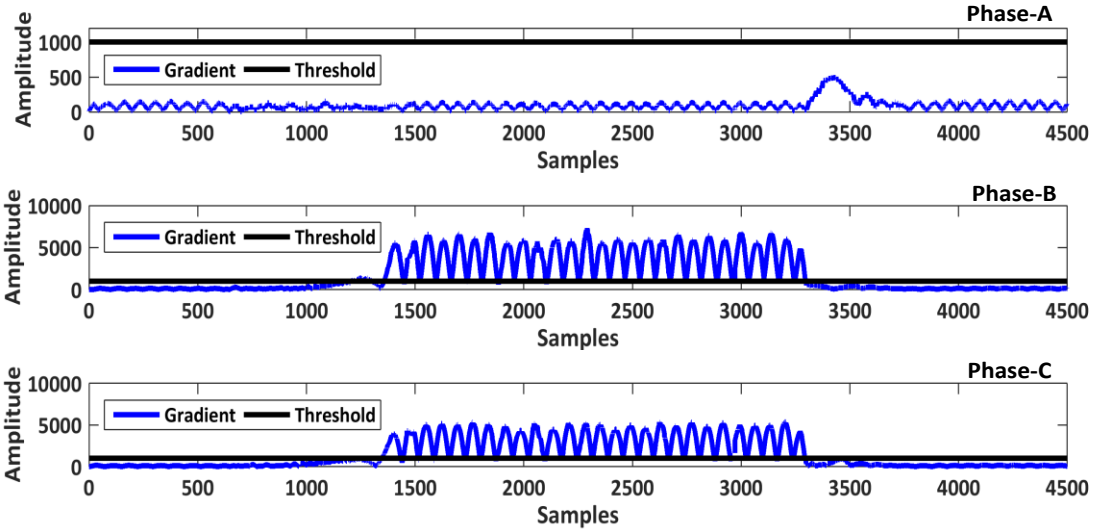

Fig. 13. Beucher gradients of phase-A, B and C currents for BCDEFG fault at 30 km, 0.07 s, R_F = 0.001 Ω and R_G = 5 Ω.

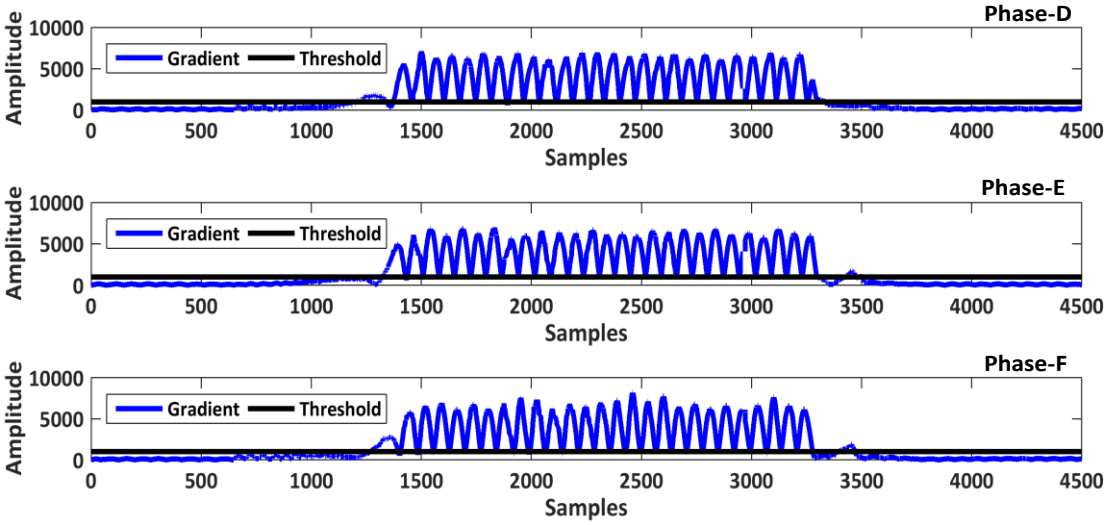

Fig. 14. Beucher gradients of phase-D, E and F currents for BCDEFG fault at 30 km, 0.07 s, R_F = 0.001 Ω and R_G = 5 Ω.

Table 4. Effectiveness of MM in detecting faults with different ground resistances.

Fault type	R_G [Ω]	FST [s]	Beucher gradients					
			Phase-A	Phase-B	Phase-C	Phase-D	Phase-E	Phase-F
BCDEFG	5	0.07	484.4866	6.8177*10^3	5.7051*10^3	7.7727*10^3	7.2932*10^3	8.5914*10^3
ABCG	15	0.07	6.9412*10^3	7.1417*10^3	6.7442*10^3	150.5955	155.4463	157.3533
DEFG	25	0.07	154.6591	154.8373	153.5161	7.1227*10^3	7.3062*10^3	6.9011*10^3
ABG	35	0.07	6.6603*10^3	5.7591*10^3	325.0294	151.7120	155.0922	153.9090
DG	45	0.07	149.9511	158.4988	151.5283	1.5139*10^3	151.5789	151.8784

4.5. Effectiveness of MM in Detecting Faults, Tested with Different FST

Here, effectiveness of the proposed MM-based scheme has been assessed for detecting different types of faults - simulated on the SPTL - with variation in FST. Fig. 15 depicts the six-phase currents for a two-phase to ground AEG fault simulated at 42 km, 0.04 s, R_F = 3.5 Ω and R_G = 4.5 Ω. Fig. 16 illustrates the Beucher gradients of phase-A, B and C currents for the AEG fault while Fig. 17 shows the Beucher gradients of phase-D, E and F currents for the AEG fault. The amplitudes of Beucher gradient of morphological filter of phase-A and E are greater than the threshold in case of AEG fault. The selected fault factors – that are common for all the fault cases - are: F_L = 42 km, FST = 0.04 s, R_F = 3.5 Ω and R_G = 4.5 Ω. Table 5 presents the results of testing the proposed MM-based scheme in detecting faults having different FST. The simulation results - depicted in Table 5 - validate the effectiveness of the proposed scheme for detecting the faults with various FST and establish that the performance of the MM-based scheme is not influenced by variation in the fault switching time.

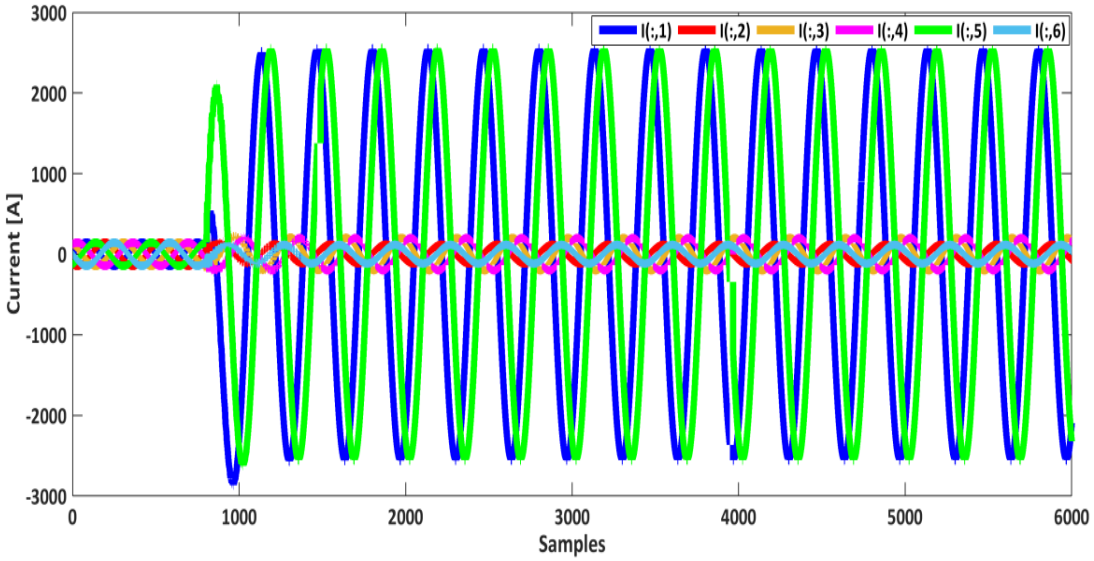

Fig. 15. Six-phase current during AEG fault at 42 km, 0.04 s, R_F = 3.5 Ω and R_G = 4.5 Ω.

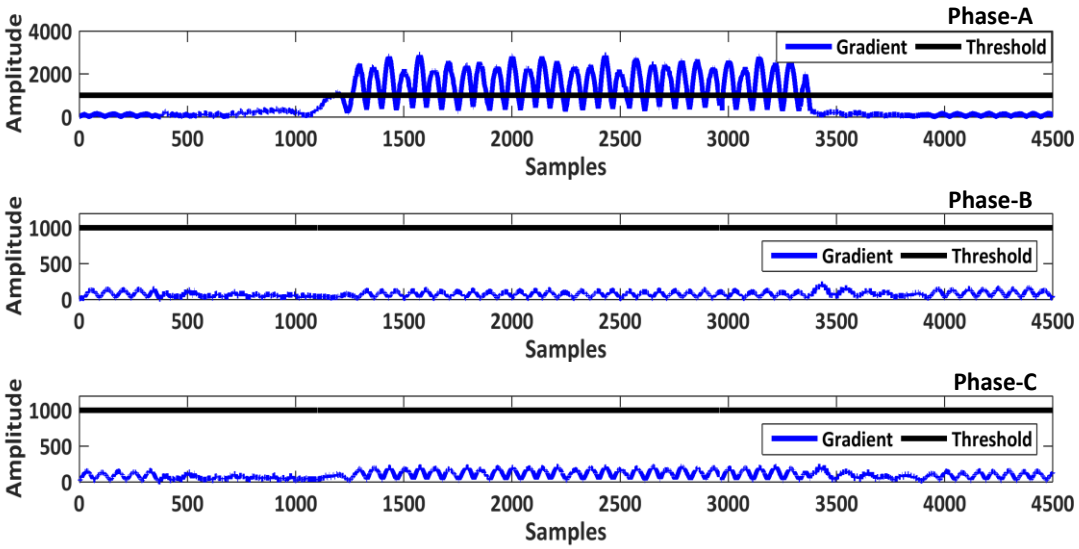

Fig. 16. Beucher gradients of phase-A, B and C currents for AEG fault at 42 km, 0.04 s, R_F = 3.5 Ω and R_G = 4.5 Ω.

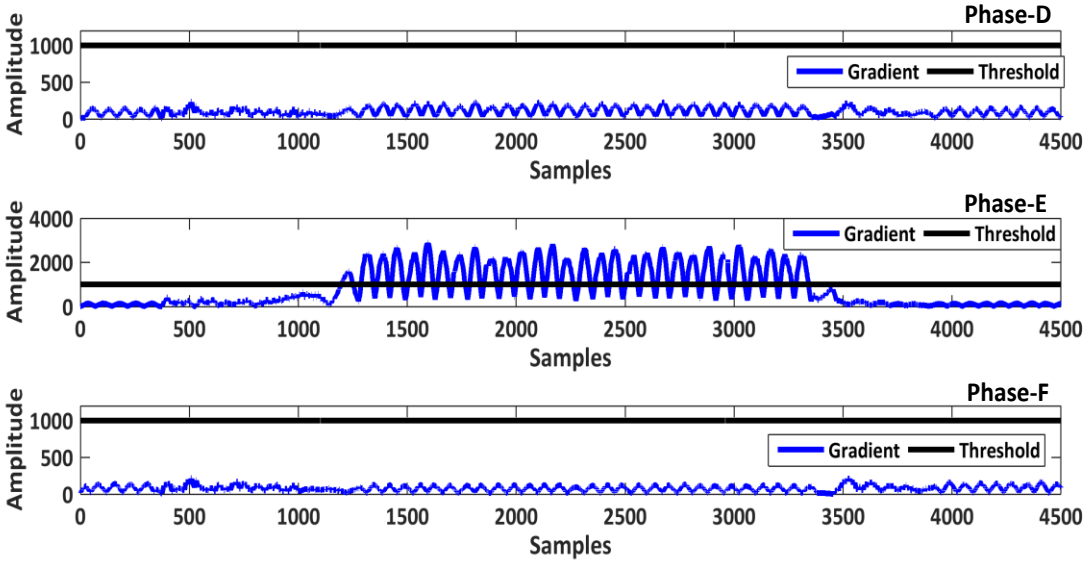

Fig. 17. Beucher gradients of phase-D, E and F currents for AEG fault at 42 km, 0.04 s, R_F = 3.5 Ω and R_G = 4.5 Ω.

Table 5. Effectiveness of MM in detecting faults with different switching times.

Fault type	FST [s]	F_L [km]	Beucher gradients					
			Phase-A	Phase-B	Phase-C	Phase-D	Phase-E	Phase-F
AEG	0.04	42	2.6479*10^3	208.6701	233.3655	242.3123	2.7080*10^3	217.1399
BCEF	0.1	42	157.9373	3.5259*10^3	3.4553*10^3	157.2192	3.4199*10^3	3.1407*10^3
ADEG	0.05	42	2.5570*10^3	206.1469	207.3008	4.1206*10^3	3.1590*10^3	456.9590
ABCDF	0.12	42	4.4915*10^3	3.8578*10^3	3.7842*10^3	3.3287*10^3	150.0613	3.5301*10^3
ACDEFG	0.08	42	3.2490*10^3	454.2107	3.6114*10^3	4.7761*10^3	3.8482*10^3	3.8025*10^3

4.6. Effectiveness of MM in Detecting Faults, Tested at Different Locations

Here, efficacy of the proposed MM-based scheme has been evaluated for different types of faults, with variation in their location. Fig. 18 depicts the six-phase currents for a most common single line to ground AG fault, simulated at 25 km, 0.06 s, R_F = 1.85 Ω and R_G = 3.85 Ω. Fig. 19 shows the Beucher gradients of phase-A, B and C currents for the AG fault. Fig. 20 illustrates the Beucher gradients of phase-D, E and F currents for the AG fault. The amplitudes of Beucher gradient of morphological filter of phase-A are greater than the threshold in case of AG fault (LG) as depicted in Fig. 19. The fault factors selected here are: FST = 0.06 s, R_F = 1.85 Ω and R_G = 3.85 Ω. Table 6 shows the results of evaluating the effectiveness of the proposed MM-based scheme in detecting different faults, tested at different locations. They authenticate the competence of MM for detecting faults with various positions on SPTL and prove that varying the fault position does not affect the performance of the proposed MM-based technique.

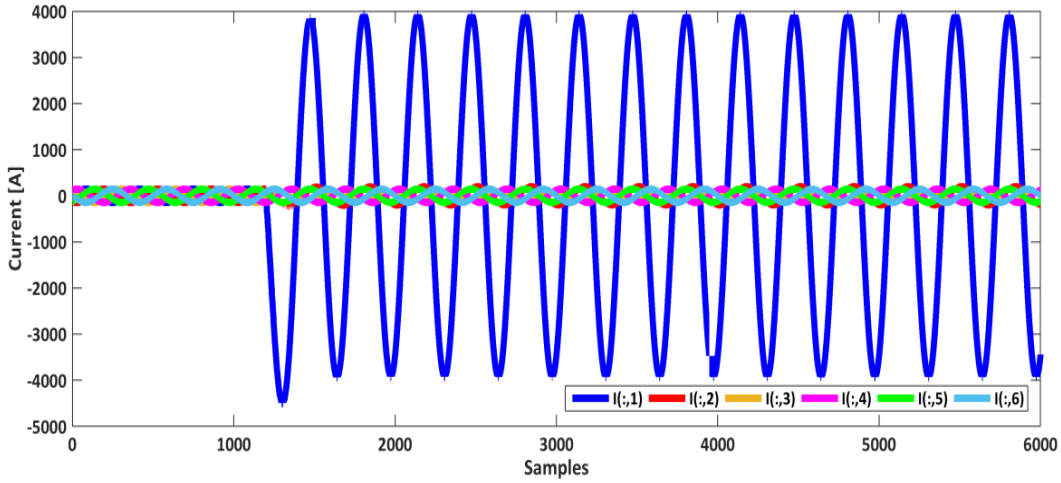

Fig. 18. Six-phase current during AG fault at 25 km, 0.06 s, R_F = 1.85 Ω and R_G = 3.85 Ω.

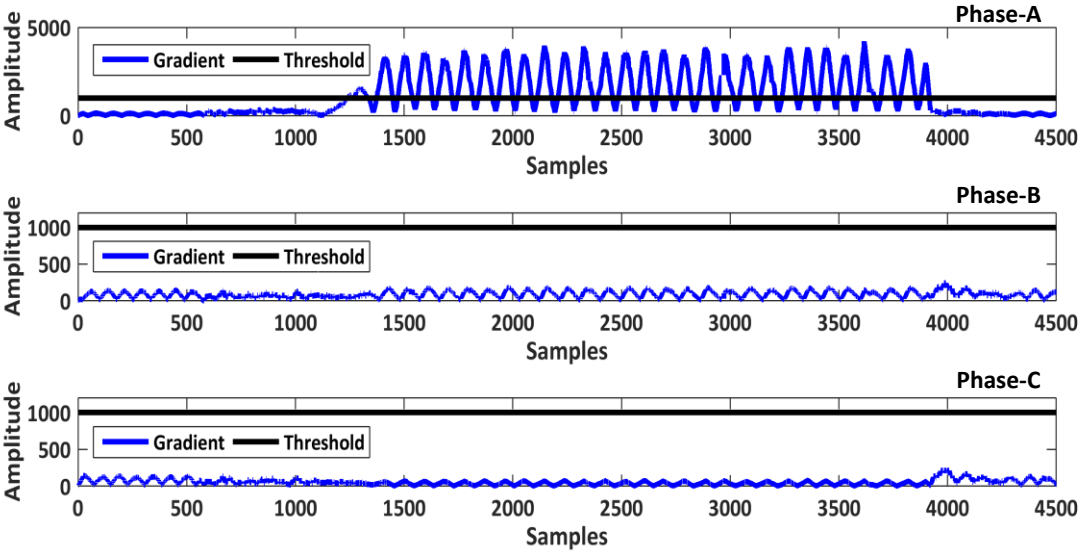

Fig. 19. Beucher gradients of phase-A, B and C currents for AG fault at 25 km, 0.06 s, R_F = 1.85 Ω and R_G = 3.85 Ω.

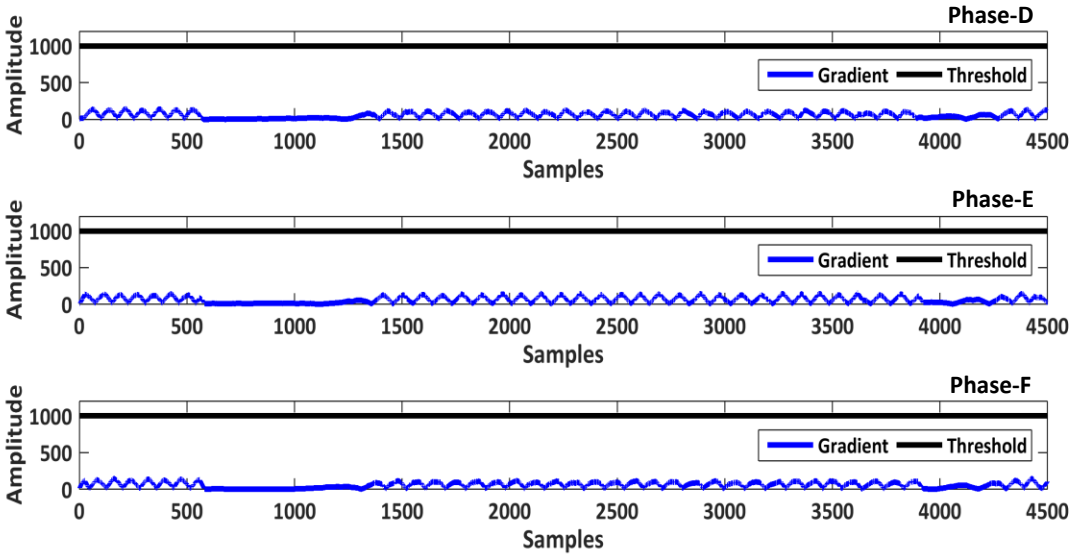

Fig. 20. Beucher gradients of phase-D, E and F currents for AG fault at 25 km, 0.06 s, R_F = 1.85 Ω and R_G = 3.85 Ω.

Table 6. Effectiveness of MM in detecting faults with various locations.

Fault type	F_L [km]	FST [s]	Beucher gradients					
			Phase-A	Phase-B	Phase-C	Phase-D	Phase-E	Phase-F
AG	25	0.06	4.0382*10^3	236.6161	210.9243	150.9603	150.9653	150.9379
DEF	30	0.06	151.2184	151.2351	151.2575	6.5064*10^3	6.7188*10^3	6.4778*10^3
ABCDG	40	0.06	5.5313*10^3	5.7586*10^3	5.3979*10^3	3.0372*10^3	228.1822	226.1464
ABCDE	45	0.06	5.5387*10^3	4.1771*10^3	4.4963*10^3	3.6131*10^3	3.6488*10^3	153.0646
ABCDEF	50	0.06	2.0005*10^3	2.1377*10^3	2.0593*10^3	2.0371*10^3	2.0272*10^3	2.0579*10^3

5. CONCLUSIONS

This work presented an enhanced explication using MM to detect and categorize faults, occurring on SPTL. The Beucher gradient of the six-phase current signals of SPTL, measured at one-end was employed by MM for fault detection, categorization and faulty phase recognition. The value of fault resistance was varied from 5 Ω to 60 Ω, the value of ground resistance was varied from 5 Ω to 45 Ω and the location of fault was varied from 25 km to 50 km. The obtained results corroborated the consistency of MM under extensive variations in fault type, location, resistance and switching time. The outcomes of this investigation revealed that there is an apparent discrimination between the fault and no-fault situations and they established the capability of the fault recognition and faulty phase categorization technique for detecting the faults correctly.

REFERENCES

[1] G. Kapoor, "Detection and classification of three phase to ground faults in a 138 kV six-phase transmission line using Hilbert-Huang transform," *JEA Journal of Electrical Engineering*, vol. 3, no. 1, pp. 11-21, 2019.

[2] V. Ashok, A. Yadav, "A real-time fault detection and classification algorithm for transmission line faults based on MODWT during power swing," *International Transactions on Electrical Energy Systems*, pp. 1-27, 2019.

[3] G. Kapoor, "Detection and classification of single line to ground boundary faults in a 138 kV six phase transmission line using Hilbert Huang transform," *i-Manager's Journal on Electrical Engineering*, vol. 12, no. 3, pp. 28-41, 2019.

[4] S. Shukla, E. Koley, S. Ghosh, D. Mohanta, "Enhancing the reliability of six-phase transmission line protection using power quality informatics with real-time validation," *International Transactions of Electrical Energy Systems*, pp. 1-21, 2019.

[5] G. Kapoor, "Protection technique for series capacitor compensated three phase transmission line connected with distributed generation using discrete Walsh Hadamard transform," *International Journal of Engineering, Science and Technology (Africa)*, vol. 11, no. 3, pp. 1-10, 2019.

[6] G. Kapoor, "Detection and classification of four phase to ground faults in a 138 kV six phase transmission line using Hilbert Huang transform," *International Journal of Engineering, Science and Technology (IJEST-Africa)*, vol. 11, no. 4, pp. 10-22, 2019.

[7] G. Kapoor, "Fifteen phase transmission line protection using daubechies-4 wavelet transform," *International Journal of Engineering, Science and Technology (IJEST-Africa)*, vol. 12, no. 1, pp. 1-14, 2020.

[8] G. Kapoor, "Wavelet transform based detection and classification of multi-location three phase to ground faults in twelve phase transmission line," *Majlesi Journal of Mechatronic Systems*, vol. 7, no. 4, pp. 47-60, 2018.

[9] E. Koley, K. Verma, S. Ghosh, "A modular neuro-wavelet based non-unit protection scheme for zone identification and fault location in six phase transmission line," *Neural Computing and Applications*, vol. 28, no. 6, pp. 1369-1385, 2017.

[10] G. Kapoor, "Six phase transmission line boundary protection using wavelet transform," *Proceedings of the 8th IEEE India International Conference on Power Electronics*, IEEE, Jaipur, India, 2018.

[11] N. Gautam, S. Ali, G. Kapoor, "Detection of fault in series capacitor compensated double circuit transmission line using wavelet transform," *Proceedings of the IEEE International Conference on Computing, Power and Communication Technologies*, pp. 769-773, IEEE, Greater Noida, India, 2018.

[12] G. Kapoor, "Fault detection of phase to phase fault in series capacitor compensated six phase transmission line using wavelet transform," *Jordan Journal of Electrical Engineering*, vol. 4, no. 3, pp. 151-164, 2018.

[13] N. Sharma, S. Ali, G. Kapoor, "Fault detection in wind farm integrated series capacitor compensated transmission line using Hilbert Huang transform", *Proceedings of the IEEE International Conference on Computing, Power and Communication Technologies*, pp. 774-778, IEEE, Greater Noida, India, 2018.

[14] G. Kapoor, "Six phase transmission line boundary protection using mathematical morphology," *Proceedings of the IEEE International Conference on Computing, Power and Communication Technologies*, pp. 857-861, IEEE, Greater Noida, India, 2018.

[15] P. Sharma, G. Kapoor, S. Ali, "Fault detection on series capacitor compensated transmission line using Walsh hadamard transform," *Proceedings of IEEE International Conference on Computing, Power and Communication Technologies*, pp. 763-768, IEEE, Greater Noida, India, 2018.